Available online at www.sciencedirect.com
SCIENCE DIRECT®
International Journal of Mass Spectrometry 232 (2004) 59–66
International Journal of Mass Spectrometry
www.elsevier.com/locate/ijms

Blackbody infrared radiative dissociation at low temperature: hydration of $X^{2+}(H_2O)_n$, for X = Mg, Ca

Richard L. Wong, Kolja Paech, Evan R. Williams*

Department of Chemistry, University of California, Berkeley, CA 94720, USA

Received 30 August 2003; accepted 24 November 2003

Abstract

A new apparatus for making blackbody infrared radiative dissociation (BIRD) measurements at below ambient temperature is described, and its use for measuring threshold dissociation energies of weakly bound clusters is demonstrated. Hydration energies are determined for alkaline-earth metal water clusters, $X^{2+}(H_2O)_n$, X = Mg, Ca and n = 8–10. For n = 8 and 9, the energies obtained from BIRD measurements are in excellent agreement with values reported previously, but for n = 10, the energies are slightly lower than those determined previously using the high-pressure ion source mass spectrometry (HPMS) equilibrium method.

Keywords: Hydration; BIRD; Binding energies; Metal ions; Dissociation

1. Introduction

In aqueous solution, the conformation of a molecule is the result of a delicate balance between intramolecular forces and forces between the molecule and water. In the gas phase, information about the intrinsic conformation of a molecule can be obtained from isolated molecules without solvent. A key difference between gas phase and solution phase interactions is the ability of water to solvate charge in solution. Because water molecules have an unusually large dipole moment and can reorient themselves along electric fields, water can attenuate the strength of electrostatic interactions by a factor of ∼80. Consequently, electrostatic interactions are markedly influenced by the presence of water molecules. In solution, water influences the strength of metal ion interactions with other molecules. For example, the regulator protein calmodulin is activated by the binding of either three or four Ca^{2+} ions [1,2]. The binding interaction between Ca^{2+} ions and calmodulin is in competition with both Ca^{2+}–water and calmodulin–water interactions. Thus, metal ion hydration studies provide not only the fundamental metal ion chemistry in water, but can also give insight for many biological reactions in which metal ion interaction plays an important role. In principle, it should be possible to examine each of these interactions individually by studying the respective hydrated ions in the gas phase.

Electrospray ionization (ESI) [3,4] is a "soft" ionization method that is well known for its ability to produce intact gas phase ions of large molecules, such as proteins [5–8], and divalent metal ions directly from solutions [9–16]. Extensively hydrated ions, both of biomolecules [17–23] and of divalent metal ions [9–16] can also be produced directly using ESI. Alternatively, hydrated ions and other solvent-attached clusters can also be formed by condensation of solvent molecules onto "naked" ions in the supersonic expansion of an electrospray interface [24,25]. Both mechanisms for hydrated ion production, solvent evaporation and condensation, can occur in ESI [18]. The ability to produce hydrated metal ions makes it possible to obtain quantitative information about the gas phase binding interactions of individual water molecules and the metal ion through equilibrium or kinetic experiments. In equilibrium experiments, such as high-pressure ion source mass spectrometry (HPMS) or low field ion mobility experiments, the enthalpy difference, ΔH, between the reactant and product states is measured from the temperature dependence of the equilibrium constant. In kinetic methods, such as blackbody infrared radiative dissociation (BIRD), the threshold dissociation energy, E_o, is determined from the temperature dependence of the unimolecular dissociation rate constant. The ΔH and E_o values can be read-

* Corresponding author. Tel.: +1-510-643-7161; fax: +1-510-642-7714.
E-mail address: williams@cchem.berkeley.edu (E.R. Williams).

1387-3806/$ – see front matter © 2003 Elsevier B.V. All rights reserved.
doi:10.1016/j.ijms.2003.11.008

ily related when the dissociation pathway has no significant reverse activation barrier. Reactions for the loss of a single water molecule are expected to have loose transition states with minimal reverse activation barriers.

Kebarle and coworkers were the first to measure the dehydration $\Delta G_{n,n-1}$ of divalent alkaline-earth metal ions formed by electrospray using HPMS equilibrium measurements [9,10]. The numbers of inner shell versus outer shell water molecules were determined by comparing experimental $\Delta H_{n,n-1}$ and $\Delta S_{n,n-1}$ values to the results of theoretical calculations [11]. The maximum number of inner shell water molecules increases with cation size. The E_o values for hydrates of divalent alkaline-earth metal ions with four to seven water molecules were measured by BIRD [14,15]. Two isomers for $Mg^{2+}(H_2O)_6$ were found to exist: one with all six water molecules in the inner shell, and one with four water molecules in the inner shell and two in the outer shell. Triply charged hydrates of metal ions have not yet been formed by electrospray. Formation of the metal hydroxide, $[XOH(H_2O)_{n-1}]^{2+}$, with loss of H_3O^+ is commonly observed [26,27].

While BIRD has been used to obtain E_o values for many biomolecules [28,29] and noncovalent complexes [30–32], including DNA duplexes [33], and protein–oligosaccharide complexes [34,35], its use has been limited to complexes that dissociate slowly or not at all at room temperature. For weakly bound complexes that dissociate rapidly at room temperature, it is difficult to obtain accurate dissociation rates at elevated temperatures. Here, we report results from a new ion cell and thermal jacket that can be either heated or cooled. The use of this new apparatus is demonstrated by measuring E_o values of alkaline-earth water clusters ions: $X^{2+}(H_2O)_n$, X = Mg, Ca; n = 8–10.

2. Experimental

2.1. Instrumentation

Experimental measurements were performed on a 2.7 T external ESI source Fourier-transform ion cyclotron resonance (FT-ICR) mass spectrometer [36]. Divalent magnesium and calcium ions are formed by nanoelectrospray using $MgCl_2$ and $CaCl_2$ solutions in which the metal ion concentration is 1×10^{-3} M. Nanoelectrospray needles are made from 1.0 mm o.d. borosilicate capillaries that are pulled to an i.d. of ~4 μm at one end using a micropipette puller (Sutter Instruments Inc., Novato, CA). Ions are guided through five stages of differential pumping into the magnetic field via a series of electrostatic lenses. Ion trapping is enhanced using nitrogen gas which is introduced through a pulsed valve to a pressure of $\sim 2 \times 10^{-6}$ Torr. After a 5 s delay, the base pressure of the vacuum chamber returns to $\sim 3 \times 10^{-9}$ Torr. Ions are isolated using multiple single frequency waveforms.

All BIRD experiments are performed with a cylindrical ion cell that is surrounded by a thermal jacket, which can be either resistively heated, or cooled by liquid nitrogen. The ion cell is 7 cm in diameter and 10 cm in length (Fig. 1, bottom). It consists of four excite/detect plates made from copper mesh to minimize their thermal mass, two macor rings that electrically isolate each of the plates from the thermal jacket and from each other, and two beryllium–copper alloy trap plates.

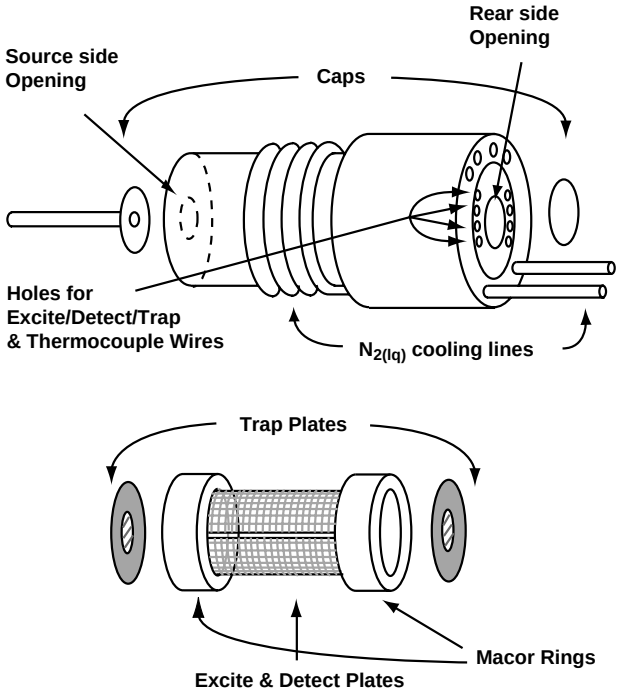

Fig. 1. Schematic diagram of the liquid nitrogen cooled thermal jacket (top) and the cylindrical FT-ICR ion cell (bottom).

The thermal jacket is made from oxygen-free copper, and it fully encloses the cell except for 10 holes shown in Fig. 1. Two of the larger openings (2.0 cm diameter and 1.5 cm diameter) are centered along the long axis of the ion cell. The excite/detect/trap wires are passed through six of the smaller holes (5 mm diameter). Thermocouple wires pass through another small hole to measure the temperature of the rear trap plate. The remaining hole is not used in this experiment. Glass tubes surround these wires to provide electrical isolation from the thermal copper jacket, and they also decrease the transmission of infrared light into the cell. The rear axial opening is blocked using a solid circular copper cap for most of the experiment (Fig. 1, top). During temperature calibration, however, the solid rear cap is replaced with one which has a 5 mm diameter hole, through which a thermocouple is introduced into the ion cell center (Fig. 2). A source-side cap is attached in front of the source-side axial opening for most of the experiments. The cap consists of a 5 cm diameter copper plate that is attached to a 0.64 cm diameter tube that is 5.1 cm long. These caps reduce the solid angle subtended by the axial opening, effectively decreasing the flux of photons from the vacuum chamber into the ion cell (Fig. 1). The two caps were removed from the ther-

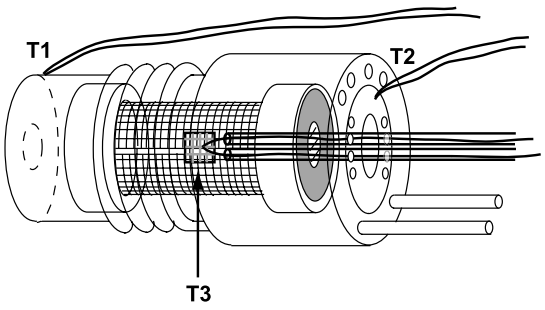

Fig. 2. Schematic diagram of the thermal jacket and ion cell showing the locations of the thermocouples: thermocouples T1 and T2 are located at opposite ends of the thermal jacket, and T3 is located in the center of the ion cell.

mal jacket during kinetic measurements made at −21 and −31 °C.

The thermal jacket is wrapped by four turns of a 0.64 cm o.d. copper tube (Fig. 1). This tube is silver-soldered to the jacket to ensure good thermal contact, and both ends of the tube are connected to the rear flange of the vacuum chamber. The thermal jacket is cooled by passing liquid nitrogen through this copper tube. The temperature of the thermal jacket is measured by a temperature-controller (Model No. CN76000, Omega Engineering, Inc., Stamford, CT), which regulates the flow of liquid nitrogen via a solenoid valve to reach and maintain a set temperature. The temperature fluctuation of the thermal jacket is less than ±1 °C, and the jacket is equilibrated for over 8 h prior to measuring cluster dissociation rates.

2.2. Modeling

At the pressures of the experiments ($<3\times10^{-9}$ Torr), collisions are so infrequent that the ion internal energy is determined by the surrounding blackbody radiation field [28]. The dissociation threshold energy, E_o, can be determined from a master equation calculation to fit the experimental dissociation rate constants and Arrhenius parameters. Details of the master equation modeling are given elsewhere [31,37].

To obtain parameters necessary for the master equation modeling, structures of the complexes are calculated. Low-energy structures of $Mg^{2+}(H_2O)_n$ and $Ca^{2+}(H_2O)_n$ (n = 7–10) were generated by using an internal coordinate Monte Carlo search with 2000 steps followed by a molecular mechanics energy minimization using the MMFFs force field in the Maestro 3.0 suite of programs (Schrödinger Inc., Portland, OR). The lowest energy structure generated from the conformation searching was then used as a starting geometry for subsequent energy minimization at the RHF/3-21 G* level using Jaguar 4.0 (Schrödinger Inc.). Vibrational frequencies and their corresponding transition dipole moments were calculated from the resulting energy minimized structures at this same computational level. The only exception was $Ca^{2+}(H_2O)_8$, for which four of the lowest energy structures (spanning an 8 kcal/mol range) generated from conformation searching were used as the starting geometries for RHF/3-21 G* calculations. Although the four structures are quite different, with anywhere from five to seven water molecules in the inner shell, the same dissociation threshold energy value, E_o, is obtained from master equation modeling using the frequency sets for any of the four structures. Similar results have been reported for isomers of $Mg^{2+}(H_2O)_n$; n = 5 and 6 [14,15], and for the three isomeric molecules, valine, betaine and alanine ethyl ester [22].

The microcanonical dissociation rate constants used in the master equation modeling were calculated using RRKM theory. The transition state frequencies were generated from the corresponding reactant frequencies by deleting one of the frequencies and altering five other frequencies. The frequencies of the transition state affect the entropy change between the reactant and transition state ($\Delta S_o^{\ddagger}$). The $\Delta S_o^{\ddagger}$ is related to the high-pressure Arrhenius frequency factor, (A^{∞}). $Mg^{2+}(H_2O)_9$ was chosen to test the dependence of E_o on the deleted frequency. For both $A^{\infty} = 10^{13}$ and 10^{18} s^{-1}, corresponding to a "neutral" and a "loose" transition state, respectively, removing either a mode at ∼1000 cm^{-1} or a mode at ∼3000 cm^{-1} results in essentially the same E_o value. As we have reported previously for weakly bound clusters [38], the E_o extracted from the master equation modeling is insensitive to which frequency is deleted for these hydrated ions. This is due to the significant depletion of the population with energies above the threshold dissociation energy. This phenomenon, and the relative insensitivity of E_o with choice of transition state are described in detail elsewhere [37,38].

3. Results and discussion

3.1. Temperature inside the ion cell

A new ion cell and a thermal jacket were built which make possible BIRD measurements at temperatures significantly above and significantly below ambient temperature. Because the thermal jacket does not fully enclose the ion cell, the photon distribution inside the ion cell is a combination of photons emitted from the thermal jacket and those radiated from the vacuum chamber. If radiation transfer outside the thermal jacket is significant, then the dissociation rate constants of ions will be a function of temperatures of both the vacuum chamber and of the thermal jacket. Consequently, the measured rate constants will be less sensitive to the temperature change of the thermal jacket than if the photon distribution inside the ion cell only depends on the temperature of the thermal jacket, resulting in artificially low values of measured activation energy, dissociation threshold energy and enthalpy (E_a, E_o and ΔH). Such deviation is expected to be more significant at reduced temperature, since the energy density in a blackbody radiation field is proportional to

the fourth power of the temperature. Heat can also transfer to the excite/detect/trap plates through their electrical connections, as these wires extend out to room temperature.

Two separate experiments are performed to determine the temperature inside the ion cell and to relate this to the temperature of the thermal jacket. In one experiment, three thermocouples are placed in different regions of the ion cell and the thermal jacket to measure any temperature gradients. In the other experiment, hydrated Mg^{2+} and Ca^{2+} clusters are used as "thermometer" ions and their dissociation kinetics are used to determine the temperature experienced by the ions.

3.2. Ion cell temperature calibration using thermocouples

The ion cell temperature was measured using three 0.025 cm diameter copper–constantan thermocouples (type T) placed at different locations as shown in Fig. 2. One thermocouple (T3) was positioned in the center of the ion cell, and two thermocouples (T1 and T2) were placed on opposite ends of the thermal jacket. A 2 cm × 1 cm copper mesh plate was folded in half and attached onto thermocouple T3 to provide an increased surface area for photon absorption and emission. The thermocouple leads were electrically isolated using glass tubes. Measurements from all three thermocouples were recorded as the temperature of the thermal jacket was reduced from 24 to −180 °C. The temperatures measured by T1 and T2 are within 0.5 °C of each other at all temperatures, indicating that the thermal jacket attains a uniform temperature. However, the temperature of T3 is increasingly higher than the thermal jacket temperature as the jacket temperature decreases. With the thermal jacket at −26 °C for 24 h, the temperature recorded by T3 is −17 °C. The deviation between the temperature of the thermal jacket and the temperature inside the ion cell can be fit to a second order polynomial function (Fig. 3).

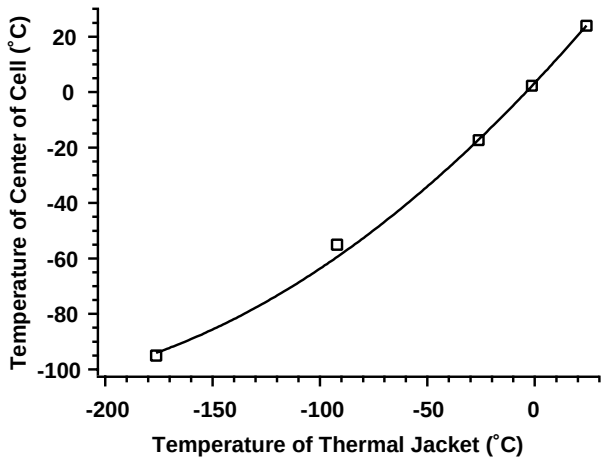

Fig. 3. Ion cell temperature calibration curve in which the temperature of the thermal jacket is plotted relative to the temperature in the ion cell center as measured by thermocouple T3. A second-order polynomial function is used to fit the data.

The higher temperature measured by T3 versus T1 and T2 can be due to (1) heat transfer to the cell center via photons or molecules leaking into the cell, (2) photons emitted from the excite/detect/trap plates that are at higher temperature than the thermal jacket due to their high thermal mass and/or heat transfer through the electrical connections, and (3) thermal conduction through the thermocouple wire itself.

For most experiments, two copper caps were placed at opposite ends of the thermal jacket to minimize the solid angle subtended by the cell axis opening at the center of the ion cell (Fig. 1). The two end-caps reduce the solid angle subtended by the opening at the center of the cell to 1.5% of its original value. This overestimates the effectiveness of the caps, because ions do not stay in the center of the cell, but rather move back and forth between the trap plates. Nevertheless, this rough estimate suggests that these end-caps significantly reduce energy transfer from external photons or molecules to the trapped ions. Fig. 4 shows the Arrhenius plots of the dehydration reactions for $X^{2+}(H_2O)_n$, X = Mg, Ca; n = 8–10 using the temperature scale derived from the thermocouple calibration. When the copper caps are removed at the two coldest thermal jacket temperatures of −21 and −31 °C, the measured dissociation rate constants do not deviate from the Arrhenius relationship with respect to the estimated ion cell temperature. The linearity of the Arrhenius plots in Fig. 4 indicates that external photons and molecules have no appreciable effect on the kinetics.

The temperature in the center of the ion cell is not only affected by photons emitted from the thermal jacket, but also the photons generated from the excite/detect/trap plates, as

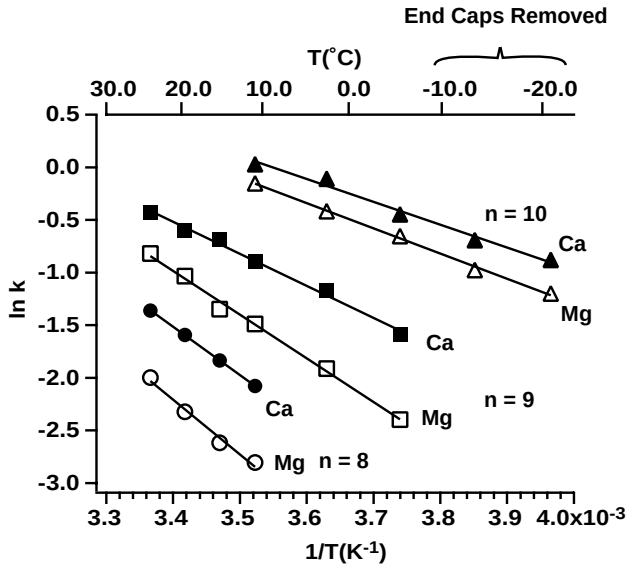

Fig. 4. Arrhenius plots of the dissociation reaction for loss of one water molecule from $X^{2+}(H_2O)_n$, X = Mg, Ca and n = 8–10 using a temperature scale that is corrected using the thermocouple calibration approach: n = 8, Mg^{2+} and Ca^{2+} water clusters (open and solid circles, respectively), n = 9, Mg^{2+} and Ca^{2+} water clusters (open and solid squares, respectively), n = 10, Mg^{2+} and Ca^{2+} waters cluster (open and solid triangles, respectively).

these plates constitute a significant fraction of the emitting surface within the ion cell (Fig. 2). These six plates have finite thermal masses and are connected by thin copper wires to feedthroughs that are at room temperature. Two experiments were conducted to investigate the extent of the heat transfer from these plates. The temperatures of the rear trap plate and thermocouple T3 (in the center of the cell) were measured as a function of time after lowering the jacket temperatures to −26 °C. After 150 min, T3 was at −5.7 °C and the rear trap plate was at −6.2 °C. After 24 h, T3 was at −17.3 °C and the trap plate was at −19.1 °C. These results show that the temperature of the trap plate is not the same as the thermal jacket temperature even after the jacket temperature is cooled for 24 h. Presumably, the temperatures of the source trap plate and mesh excite/detect plates are similar to that of the rear trap plate since they have comparable mass. The temperature of T3 remains closer to temperature of the trap plate than to the thermal jacket temperature throughout the cooling process.

In a separate experiment, the copper mesh excite/detect plates were replaced with thicker solid plates that had approximately seven times the mass of the mesh plates. The wires to the excite/detect plates were also replaced with thicker wires. After the thermal jacket was cooled to −26 °C for 150 min, the temperature of T3 was 18.3 °C and the rear trap plate was 4.3 °C. This result shows that the cooling rate of both the rear trap plate and the cell center are slowed down by the use of the thick solid plates. Results of both experiments clearly show that the temperature of excite/detect/trap plates is not equal to that of the thermal jacket even after 24 h temperature equilibration, and that the temperature in the center of the ion cell is influenced by the temperature of these ion cell plates.

From this testing, we conclude that the ion cell center (T3) is warmer than the thermal jacket (T1 and T2) mainly due to photon energy transfer from the warmer excite/detect/trap plates, and that the effect of externally generated photons and molecules leaking into the thermal jacket is small by comparison. Heat can also transfer through the thermocouple wire of T3, causing T3 to be warmer than its surroundings, but this deviation is likely to be small.

3.3. Hydration energies of $X^{2+}(H_2O)_n$, X = Mg and Ca

In order to evaluate the accuracy of the thermocouple calibration method, the dissociation of $X^{2+}(H_2O)_n$, X = Mg and Ca; n = 8–10, is investigated at low temperatures via BIRD. The dehydration enthalpies ($\Delta H_{n,n-1}$) of these divalent alkaline-earth metal water clusters have been determined by Kebarle and coworkers using a HPMS equilibrium determination method [11]. Threshold dissociation energies obtained by BIRD and those determined from HPMS experiment provide an opportunity to compare the two methods.

Dehydration rate constants of $Mg^{2+}(H_2O)_n$ and $Ca^{2+}(H_2O)_n$, n = 8–10, were measured with the thermal jacket temperature between 24 and −31 °C. Because ions are trapped in the center of the cell, the measured dehydration rate constants are determined by the photon distribution in that region. The data in Fig. 3 is used to relate the temperature of the jacket to the temperature the ions experience inside the cell. Arrhenius plots using these ion cell temperatures are shown in Fig. 4.

From the Arrhenius plots in Fig. 4, it is possible to derive E_o values via master equation modeling. Parameters in the modeling, including the high-pressure Arrhenius frequency factor, A^∞, and E_o values are varied to fit the experimental data. The criteria for a suitable fit is that the calculated values of E_a and A are within one standard deviation of the corresponding experimental values, and the calculated dissociation rate constants, k, are within a factor of two of the experimental values. Loss of water can have a range of transition state entropies. A neutral transition state of $A^\infty = 10^{13}\,s^{-1}$ and a very loose transition state $A^\infty = 10^{18}\,s^{-1}$ are selected for master equation modeling. Assuming that there is no reverse activation barrier, $\Delta H_{n,n-1}$ at temperature T can be obtained from the E_o from the following relationship [38,39]:

$$\Delta H_{n,n-1}(T) = E_o + E_{vib}(P, T) - E_{vib}(R, T) + 4RT \quad (1)$$

where $E_{vib}(P, T)$ is the average vibrational energy of all products at temperature T, and $E_{vib}(R, T)$ is the average vibrational energy of the reactant at temperature T.

Table 1 lists $\Delta H_{n,n-1}$ values at 298 K obtained from previous HPMS equilibrium measurements [11] and from these BIRD measurements. The values of $\Delta H_{8,7}$ for $Mg^{2+}(H_2O)_8$ and for $Ca^{2+}(H_2O)_8$ determined from these BIRD experiments are 0.82 ± 0.08 eV and 0.76 ± 0.06 eV, respectively. Values of 0.78 ± 0.04 eV and 0.70 ± 0.04 eV, respectively, were reported by Kebarle and coworkers. These ΔH values determined by the two methods agree within the experimental uncertainty. Similarly, the $\Delta H_{9,8}$ values obtained by BIRD agree within experimental error with those determined using the HPMS equilibrium method. For $Mg^{2+}(H_2O)_9$, $\Delta H_{9,8}$ from BIRD is 0.74±0.06 eV and 0.73±0.04 eV from HPMS. For $Ca^{2+}(H_2O)_9$, $\Delta H_{9,8}$ determined from BIRD measurement is 0.67 ± 0.06 eV and 0.66 ± 0.04 eV using the HPMS equilibrium method.

However, the values of $\Delta H_{10,9}$ obtained by the two methods do not agree. The BIRD derived $\Delta H_{10,9}$ value of $Mg^{2+}(H_2O)_{10}$ is 0.55 ± 0.04 eV, whereas the value reported by Kebarle and coworkers is 0.68 ± 0.04 eV. Similarly, the values of $\Delta H_{10,9}$ for $Ca^{2+}(H_2O)_{10}$ obtained by BIRD and HPMS are 0.51 ± 0.06 eV and 0.63 ± 0.04 eV, respectively. Multiplying the transition dipole moments for $Mg^{2+}(H_2O)_{10}$ and $Ca^{2+}(H_2O)_{10}$ by factors of 0.5 and 1.5 in the master equation resulted in no fits, indicating that the deviation in the results from these two methods for n = 10 is not due to error in calculated radiation rate constants. Since the temperature range used to acquire the n = 9 clusters data overlaps with that of the n = 10 clusters, it is surprising that the BIRD results for n = 9 clusters fit so

Table 1
Measured zero-pressure limit Arrhenius activation energies, derived dissociation threshold energy values, and dehydration enthalpy values (in eV)

	E_a	E_o	ΔH_{BIRD}[a]	ΔH_{HPMS}[a,b]	Theoretical
$Mg^{2+}(H_2O)_8$	0.45 ± 0.04	0.79 ± 0.08	0.82 ± 0.08	0.78 ± 0.04	0.66[c]
$Mg^{2+}(H_2O)_9$	0.36 ± 0.01	0.70 ± 0.06	0.74 ± 0.06	0.73 ± 0.04	
$Mg^{2+}(H_2O)_{10}$	0.205 ± 0.005	0.54 ± 0.04	0.55 ± 0.04	0.68 ± 0.04	
$Ca^{2+}(H_2O)_8$	0.395 ± 0.005	0.73 ± 0.05	0.76 ± 0.06	0.70 ± 0.04	0.38[d], 0.88[e]
$Ca^{2+}(H_2O)_9$	0.26 ± 0.01	0.63 ± 0.06	0.67 ± 0.06	0.66 ± 0.04	0.59[e]
$Ca^{2+}(H_2O)_{10}$	0.185 ± 0.015	0.51 ± 0.06	0.51 ± 0.06	0.63 ± 0.04	

[a] All ΔH values are enthalpy changes at standard state 1 atm at 298 K.
[b] From reference [11]. Successive water binding energy calculated using DFT B3LYP by Pavlov et al. [40].
[c] $[Mg^{2+}(H_2O)_6](H_2O)_2$.
[d] $Ca^{2+}(H_2O)_8$.
[e] Successive hydration enthalpies at 298 K calculated using MP2 by Katz et al. [41].

well with the HPMS equilibrium results while the results for the $n = 10$ clusters do not.

3.4. Ion cell temperature calibration using thermometer ions

From the previously reported values of hydration enthalpies of alkaline-earth metal ions, it is possible to obtain a temperature from the zero-pressure kinetics by doing essentially the reverse process in the master equation modeling. Namely, T is varied in the modeling while E_o is fixed at the previously measured value. Values of E_o are determined from $\Delta H_{n,n-1}$ values obtained from HPMS equilibrium experiments via Eq. (1) [11]. Using these E_o values, zero-pressure activation energy values, E_a, are calculated from master equation modeling using frequency sets corresponding to both $A^\infty = 10^{13}$ and $10^{18}\,s^{-1}$. The temperature scale is varied until the resulting zero-pressure Arrhenius parameters match those calculated from the master equation modeling (Table 2). A third-order polynomial function is used to fit the ion cell temperature derived in this way to the thermal jacket temperature. Arrhenius plots using the temperatures derived from the "thermometer ion calibration" are shown in Fig. 5. The Arrhenius data for the $X^{2+}(H_2O)_n$, X = Mg, Ca and $n = 9$, 10 has curvature at the lower temperatures.

In addition to the curvature in the Arrhenius plots using the thermometer ion calibration scale (Fig. 5), a wide range of transition state entropies are required to fit the experimental E_a values to HPMS results. For both $Mg^{2+}(H_2O)_8$ and $Ca^{2+}(H_2O)_8$, significantly lower values of A^∞ are necessary to fit the experimental results than are required for $Mg^{2+}(H_2O)_{10}$ and $Ca^{2+}(H_2O)_{10}$. For example, the experimental E_a value of $Ca^{2+}(H_2O)_8$ using the thermometer ion calibration is 0.40 eV. The calculated E_a values are 0.42 eV for $A^\infty = 10^{13}\,s^{-1}$ and 0.31 eV for $A^\infty = 10^{18}\,s^{-1}$. Thus, a "neutral" transition state is required to fit the data. For $Mg^{2+}(H_2O)_{10}$, the experimental E_a using the thermometer ion calibration is 0.30 eV, and the calculated values of E_a are 0.40 eV for $A^\infty = 10^{13}\,s^{-1}$ and 0.31 eV for $A^\infty = 10^{18}\,s^{-1}$. Thus, a very "loose" transition state is required to fit the data.

The large difference in transition state entropies required to fit the data is much greater than expected based on the $\Delta(\Delta S)$ values measured by the HPMS equilibrium method [11]. In the HPMS equilibrium experiments, the difference in the dehydration entropy between $\Delta S_{10,9}$ and $\Delta S_{8,7}$ for

Table 2
Calculated zero-pressure Arrhenius parameters

	A^∞	Zero-pressure Arrhenius parameters calculated using			
		HPMS equilibrium results[a]		Thermometer ion temperature calibration	
		E_a (eV)	A (s^{-1})	E_a (eV)	A (s^{-1})
$Mg^{2+}(H_2O)_8$	10^{13}	0.54	$10^{7.7}$	0.46	$10^{6.9}$
	10^{18}	0.39	$10^{6.0}$		
$Mg^{2+}(H_2O)_9$	10^{13}	0.46	$10^{7.0}$	0.40	$10^{6.4}$
	10^{18}	0.32	$10^{5.2}$		
$Mg^{2+}(H_2O)_{10}$	10^{13}	0.40	$10^{6.2}$	0.30	$10^{5.3}$
	10^{18}	0.31	$10^{5.1}$		
$Ca^{2+}(H_2O)_8$	10^{13}	0.42	$10^{6.3}$	0.40	$10^{6.3}$
	10^{18}	0.31	$10^{5.0}$		
$Ca^{2+}(H_2O)_9$	10^{13}	0.33	$10^{5.2}$	0.29	$10^{4.7}$
	10^{18}	0.23	$10^{4.0}$		
$Ca^{2+}(H_2O)_{10}$	10^{13}	0.35	$10^{5.6}$	0.27	$10^{4.8}$
	10^{18}	0.24	$10^{4.3}$		

[a] From reference [11].

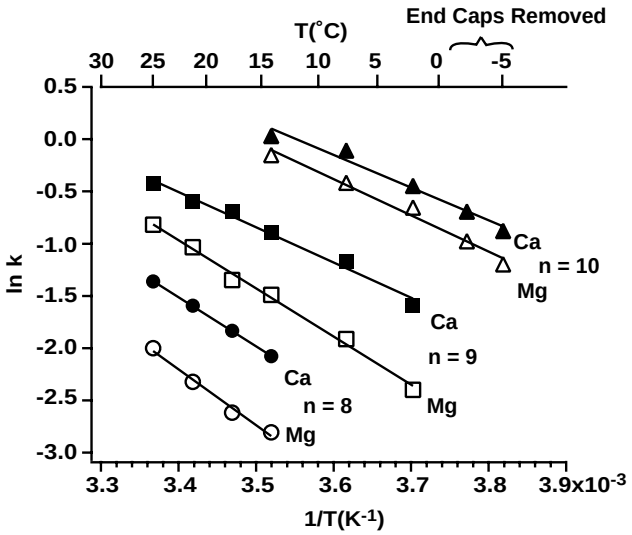

Fig. 5. Arrhenius plots of the dissociation reaction for loss of one water molecule from $X^{2+}(H_2O)_n$, X = Mg, Ca and n = 8–10 using a temperature scale that is corrected using the thermometer ion calibration method: n = 8, Mg^{2+} and Ca^{2+} water clusters (open and solid circles, respectively), n = 9, Mg^{2+} and Ca^{2+} water clusters (open and solid squares, respectively), n = 10, Mg^{2+} and Ca^{2+} waters cluster (open and solid triangles, respectively).

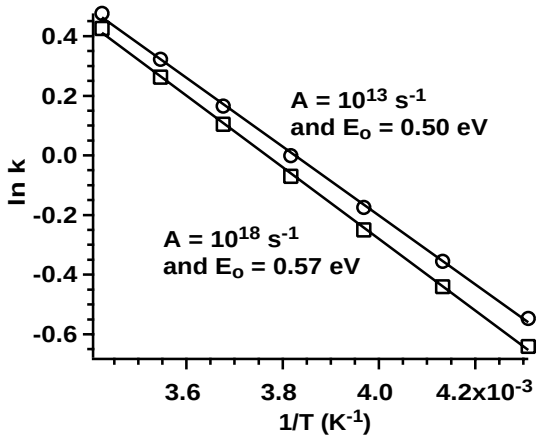

Fig. 6. Simulated low-pressure Arrhenius plots using master equation modeling with $A = 10^{13}\,s^{-1}$ and $E_o = 0.50$ eV (open circles), and $A = 10^{18}\,s^{-1}$ and $E_o = 0.57$ eV (open squares).

both calcium and magnesium is about 2 cal/K mol. From the thermodynamic formulation of transition state theory, the relationship between A^∞ and entropy change between the reactant and transition state ($\Delta S_o^\ddagger$) is:

$$A^\infty = \frac{k_B T}{h} e^{(1+(\Delta S_o^\ddagger/R))} \quad (2)$$

where k_B is the Boltzmann constant, T is the temperature, h is the Plank constant, and R is the ideal gas constant. The $\Delta(\Delta S)$ value of 2.0 cal/K mol corresponds to a $\Delta(\log A^\infty) = 0.43$ between the two dehydration processes. This difference is significantly smaller than the difference of A^∞ ($\Delta(\log A^\infty) = 5$) required to fit the zero-pressure kinetic data to the ΔH values obtained from the HPMS equilibrium data.

It should be noted that ΔS measured by the HPMS equilibrium experiment is the entropy difference between reactant and final products, whereas the A^∞ value measured in a BIRD experiment is a function of entropy difference between the reactant and transition state. The measured difference in entropies for $n = 8$ versus $n = 10$ should be even smaller in the BIRD experiment than in the HPMS equilibrium experiment.

3.5. Discrepancy in the temperature calibration methods

The origin of the difference in the ion cell temperature calibration using the thermocouple versus thermometer ion method at the lower temperatures is not entirely clear. The thermometer ion method and thermocouple method provide similar results at the higher temperatures, and thus provide similar values of E_a for the hydrates with eight or nine water molecules. However, the temperature scale obtained from the thermometer ion method is compressed at the lower temperatures to provide a higher value of E_a for the hydrates with 10 water molecules (Figs. 4 and 5), which produces curvature in the Arrhenius data where there should be none and an unusually wide range of transition state entropies are required to model the data with this "thermometer ion calibration" scale.

To confirm that there should be no curvature in the Arrhenius plots at low temperatures, the dissociation of $Mg^{2+}(H_2O)_{10}$ was modeled using master equation modeling at two sets of dissociation parameters: (1) $A^\infty = 10^{13}\,s^{-1}$ and $E_o = 0.50$ eV, (2) $A^\infty = 10^{18}\,s^{-1}$ and $E_o = 0.57$ eV. The resulting Arrhenius plots are both linear (Fig. 6).

It should be noted that the values of ΔH we report are obtained from the derived values of E_o and are the differences between the reactant and transition states, assuming no reverse activation barrier. On the other hand, the ΔH values from HPMS are the differences between reactants and products. If a reverse activation barrier was present, the $\Delta H_{n,n-1}$ values we report would be too high. Just the opposite is indicated using the temperature calibration derived from thermocouple measurements (Table 1).

If the temperature calibration using the thermometer ion is correct, then the temperature of the thermocouple inside the cell (T3) must be lower than that experienced by the ions. However, any expected thermometer calibration error such as heat conduction through the thermocouple wires or non-equilibrated temperature reading can only make T3 reports a higher temperature than the true temperature in the ion cell center, not lower. The heat conduction through the thermocouple wires is not expected to be significant. Otherwise, all ΔH values obtained from BIRD would deviate from those obtained using HPMS.

This combination of factors leads us to believe that the temperature scale derived from the thermocouple measure-

ments is more accurate, and that the $\Delta H_{n,n-1}$ values measured by Kebarle for $Mg^{2+}(H_2O)_{10}$ and $Ca^{2+}(H_2O)_{10}$ are high. It should be noted that the magnitude of the difference, $\leq$0.13 eV, although outside the reported experimental uncertainty of the two methods (0.04–0.06 eV), is relatively small.

4. Conclusions

The use of a new apparatus for making BIRD measurements is demonstrated. This apparatus consists of a cylindrical ion cell and a thermal jacket that can be cooled with liquid nitrogen or resistively heated. Two calibration methods are used to relate the temperature of the thermal jacket to the temperature inside the ion cell. In one method, two thermocouples are placed at different locations on the thermal jacket and a third thermocouple is placed in the center of the ion cell. From the thermocouple measurements, a calibration curve relating the temperature of the thermal jacket to the temperature inside the cell is obtained. In the other method, hydrated alkaline-earth metal clusters $X^{2+}(H_2O)_n$, X = Mg, Ca and n = 8–10, are used as "thermometer ions." A temperature scale is obtained by fitting the scale used in the master equation modeling until the hydration enthalpies fit those reported previously. The thermocouple calibration appears to be a more reliable approach. Using the thermocouple calibration temperature scale, the measured dehydration enthalpies of $X^{2+}(H_2O)_n$, X = Mg, Ca, n = 8 and 9 are in excellent agreement with previously reported values. However, for n = 10, dehydration enthalpies measured via BIRD are lower ($\leq$0.13 eV) than previously reported via HPMS measurements. We believe that the values reported here are more accurate.

Acknowledgements

The authors would like to acknowledge Dr. Rebecca A. Jockusch for her assistance in the ab initio calculations. This research would not have been possible if not for the generous financial support provided by National Science Foundation (grant CHE-0098109).

References

[1] T.E. Creighton, Proteins, 2nd ed., W.H. Freeman & Co., New York, 1993.
[2] L. Stryer, Biochemistry, 4th ed., W.H. Freeman & Co., New York, 1995.
[3] M. Yamashita, J.B. Fenn, J. Phys. Chem. 88 (1984) 4671.
[4] J.B. Fenn, M. Mann, C.K. Meng, S.F. Wong, C.M. Whitehouse, Science 246 (1989) 64.
[5] J.A. Loo, C.G. Edmonds, R.D. Smith, Anal. Chem. 63 (1991) 2488.
[6] D.F. Hunt, R.A. Henderson, J. Shabanowitz, K. Sakaguchi, H. Michel, N. Sevilir, A.L. Cox, E. Appella, V.H. Engelhard, Science 255 (1992) 1261.
[7] A. Miranker, C.V. Robinson, S.E. Radford, R.T. Aplin, C.M. Dobson, Science 262 (1993) 896.
[8] G.A. Valaskovic, N.L. Kelleher, F.W. McLafferty, Science 273 (1996) 1199.
[9] A.T. Blades, P. Jayaweera, M.G. Ikonomou, P. Kebarle, J. Chem. Phys. 92 (1990) 5900.
[10] A.T. Blades, P. Jayaweera, M.G. Ikonomou, P. Kebarle, Int. J. Mass Spectrom. Ion Process. 102 (1990) 251.
[11] M. Peschke, A.T. Blades, P. Kebarle, J. Phys. Chem. A 102 (1998) 9978.
[12] M. Peschke, A.T. Blades, P. Kebarle, Int. J. Mass Spectrom. 187 (1999) 685.
[13] M. Peschke, A.T. Blades, P. Kebarle, J. Am. Chem. Soc. 122 (2000) 10440.
[14] S.E. Rodriguez-Cruz, R.A. Jockusch, E.R. Williams, J. Am. Chem. Soc. 120 (1998) 5842.
[15] S.E. Rodriguez-Cruz, R.A. Jockusch, E.R. Williams, J. Am. Chem. Soc. 121 (1999) 1986.
[16] S.E. Rodriguez-Cruz, E.R. Williams, J. Am. Soc. Mass Spectrom. 12 (2000) 250.
[17] S.E. Rodriguez-Cruz, J.S. Klassen, E.R. Williams, J. Am. Soc. Mass Spectrom. 8 (1997) 565.
[18] S.E. Rodriguez-Cruz, J.S. Klassen, E.R. Williams, J. Am. Soc. Mass Spectrom. 10 (1999) 958.
[19] S.-W. Lee, P. Freivogel, T. Schindler, J.L. Beauchamp, J. Am. Chem. Soc. 120 (1998) 11758.
[20] J.S. Klassen, A.T. Blades, P. Kebarle, J. Phys. Chem. 99 (1995) 15509.
[21] A.T. Blades, J.S. Klassen, P. Kebarle, J. Am. Chem. Soc. 118 (1996) 12437.
[22] R.A. Jockusch, A.S. Lemoff, E.R. Williams, J. Am. Chem. Soc. 123 (2001) 12255.
[23] R.A. Jockusch, A.S. Lemoff, E.R. Williams, J. Phys. Chem. A 105 (2001) 10929.
[24] T. Spence, T.D. Burns, L.A. Posey, J. Phys. Chem. A 101 (1997) 139.
[25] D. Zhan, J. Rosell, J.B. Fenn, J. Am. Soc. Mass Spectrom. 9 (1998) 1241.
[26] A.T. Blades, P. Jayaweera, M.G. Ikonomou, P. Kebarle, Int. J. Mass Spectrom. Ion Process. 101 (1990) 325.
[27] D. Vukomanovic, J.A. Stone, Int. J. Mass Spectrom. 202 (2000) 251.
[28] W.D. Price, P.D. Schnier, R.A. Jockusch, E.F. Strittmatter, E.R. Williams, J. Am. Chem. Soc. 118 (1996) 10640.
[29] R.A. Jockusch, P.D. Schnier, W.D. Price, E.F. Strittmatter, P.A. Demirev, E.R. Williams, Anal. Chem. 69 (1997) 1119.
[30] R.C. Dunbar, T.B. McMahon, D. Tholmann, D.S. Tonner, D.R. Salahub, D. Wei, J. Am. Chem. Soc. 117 (1995) 12819.
[31] W.D. Price, P.D. Schnier, E.R. Williams, J. Phys. Chem. B 101 (1997) 664.
[32] S.M. Stevens Jr., R.C. Dunbar, W.D. Price, M. Sena, C.H. Watson, L.S. Nichols, J.M. Riveros, D.E. Richardson, J.R. Eyler, J. Phys. Chem. A 106 (2002) 9686.
[33] P.D. Schnier, J.S. Klassen, E.F. Strittmatter, E.R. Williams, J. Am. Chem. Soc. 120 (1998) 9605.
[34] E.N. Kitova, D.R. Bundle, J.S. Klassen, J. Am. Chem. Soc. 124 (2001) 5902.
[35] E.N. Kitova, D.R. Bundle, J.S. Klassen, J. Am. Chem. Soc. 124 (2002) 9340.
[36] D.S. Gross, E.R. Williams, J. Am. Chem. Soc. 117 (1995) 883.
[37] W.D. Price, E.R. Williams, J. Phys. Chem. A 101 (1997) 8844.
[38] R.A. Jockusch, E.R. Williams, J. Phys. Chem. 102 (1998) 4543.
[39] N.F. Dalleska, K. Honma, P.B. Armentrout, J. Am. Chem. Soc. 115 (1993) 12125.
[40] M. Pavlov, P.E.M. Siegbahn, M. Sandstrom, J. Phys. Chem. A 102 (1998) 219.
[41] A.K. Katz, J.P. Glusker, S.A. Beebe, C.W. Bock, J. Am. Chem. Soc. 1996 (1996) 5752.